Real-time simulation Model of Ultracapacitors for Frequency Stability Support from Wind Generation

C. Zhang [(1)], E. Rakhshani [(1)], N. Veera Kumar [(1)], J.L. Rueda-Torres [(1)], P. Palensky [(1)], F. Gonzalez-Longatt[(2)]
[(1)] Department of Electrical Sustainable Energy, Delft University of Technology, Netherlands
[(2)] Department of Electrical Engineering, Information Technology and Cybernetics, University of South-Eastern Norway, Norway
rakhshani@ieee.org, J.L.RuedaTorres@tudelft.nl

***Abstract*— The frequency stability of the power system is challenged by the high penetration of power electronic interfaced renewable energy sources (RES). Energy storage systems (ESS) are used to supply extra power injection to enhance the frequency stability during a disturbance. This paper presents a novel approach for improving the frequency dynamics by incorporating a designed ultracapacitor (UC) with a fully decoupled wind power generation (FDWG) unit. To this aim, a suitable model implementation of UC for real-time simulations is presented. The model constitutes a parallel RC branch, which is appropriate for illustrating the relevant fast UC dynamics that occur within the first milliseconds of the time period of action for fast active-power frequency control services. The frequency performance achieved by the support of the FDWG equipped with UC is compared against the performance achieved by using electrical batteries. The comparison includes the application of droop-derivative frequency control.**

Keywords*— *Fast active power-frequency control ultracapacitor model, RTDS, fully decoupled wind power generator

I. INTRODUCTION

Due to the societal ambition of a 100% clean power supply for increasing electrical demands, the constitution of energy sources in the power system is predominantly growing towards massive integration of renewable energy sources (RES), e.g. wind power generators. Traditionally, the frequency stability of the power system is supported by the inertia response of heavy rotating machinery like conventional synchronous generators [1]. However, the inherent inertia of renewable power generators is significantly smaller, and it is decoupled from the power system due to their power converter-based interconnection [2]. Up to now, several research activities are reported presenting different approaches on inertia control techniques in high-penetrated wind generator grids and their challenges [3]-[7]. These approaches are mainly focused on de-loading operation mode of wind turbines [3],[4] or methods based on releasing the kinetic energy of the unit [5],[6]. Considering the technical limitation for proper operation of these kinds of methods, incorporation of hybrid energy storage technologies was also presented as a complementary source of energy for such wind-based generation unit [7]-[9]. Thanks to these proposed hybrid solutions with storage technologies, the operational limitation of wind turbine is improved by providing additional source of energy. But, as indicated in recent reports, additional consideration at the modelling and design stage have been missed. For example, in [7] more technical details, such as dynamic characteristics of power source, power and rotor limitations of wind turbine, for accurate performance could be considered. Whereas, in [8], there is a lack of technical detail of UC model for proper representation of the operation during charging process. Hence, to enhance the frequency stability of the power system, the consideration of supplementary power sources and frequency control methods should be investigated to determine effective means to prevent and mitigate undesirable dynamic frequency excursions that can lead to instability. For the first aspect, for instance, the most widely studied solution is the addition of electrical batteries [10]. Nevertheless, since the rate-of-change-of-frequency (ROCOF) and the maximum frequency deviation in a low inertia system can be significantly high, and they can happen within a reduced time frame, further research is needed to determine effective and fast-reacting solutions [11]. This gap must be filled with more adequate modelling of UC considering its real-time operation.

This paper concerns the modelling of an ultracapacitor (UC) based energy storage system (ESS), which is integrated into a model of a wind power generator for the design and study of fast active power-frequency control. The UC has a higher power density and faster-reacting speed than a traditional solution with electrical batteries. The model of the UC is implemented in RSCAD (a software package used for real-time digital simulation), and it allows the representation of the dynamic behaviour of the distributed circuit elements, the charge redistribution, and voltage-dependent impedance. The UC model is used to enhance the frequency response of fully decoupled wind power generators (FDWGs), which are added into a modified IEEE 9 bus test system to simulate challenging operating conditions with reduced inertia and steep values of ROCOF and maximum frequency deviation. The simulation results obtained by using the UCs are qualitatively compared against the results obtained by using electrical batteries to reflect on the extent of enhanced mitigation of both ROCOF and maximum frequency deviation.

The remainder of the paper is structured as follows: Section 2 overviews the fundamental principles behind UC and its fast dynamic response. Section 3 discusses the modelling approaches for UC. Section 4 presents the implemented model in RSCAD. Section 5 show the obtained numerical results. Finally, Section 6 summarizes the concluding remarks.

II. RATIONALE BEHIND UC

A typical UC structure is formed by two porous electrodes, an inner electrolyte and two current collectors. When external energy sources charge the UC, current collectors help to accumulate positive and negative charges on the two electrodes. Fig. 1 shows the inner structure of a charged UC. The electrolyte is filled between the two electrodes. The cations and anions in the electrolyte are attracted by the charged electrodes. Usually, the electrodes are made of carbon with numerous pores. The attracted cations and anions in the porous electrodes forming distributed electric fields. In contrast, a normal parallel plate capacitor has a non-conducting material like air between two electrodes. The charges are only distributed on the surface of the parallel electrodes, and the strength of the electric field depends on the dielectric strength.

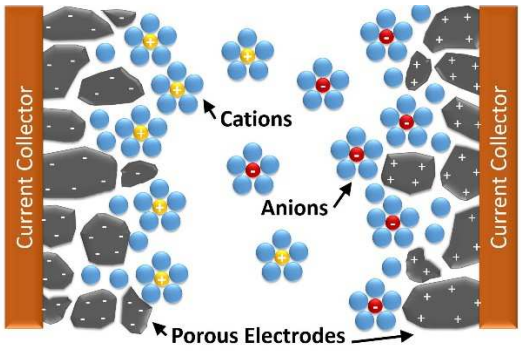

Fig. 1. Porous structure of an ultracapacitor (inspired by [5]).

Comparing with parallel plate capacitors, UCs have significantly improved the electrodes' area $1000 - 2000 m^2/cm^3$ [12]. Besides, the particle-scale electric fields are formed in porous electrodes, so the small distance of the electric field also increases the capacitance of UC. Since UCs have different structures from parallel plate capacitors, some dynamic performance of UCs is also different from normal capacitors. In order to build detailed UC models, the dynamic properties of UCs should be considered in the following aspects:

1) Distributed circuit elements: Unlike in parallel plate capacitors, where charges are distributed on the surface of the electrodes, the porous structures of UC electrodes contain more distributed charges forming numerous particle-scale electric fields. This structure increases the effective area and decreases the distance between heterogeneous electrodes, which significantly increases the capacitance of UC. In order to model this distributed structure, partial capacitance and partial resistance need to be concerned [12].

2) Charge redistribution phenomenon: The diffusion ions travel a time in the electrolyte into the porous electrodes leading to a spontaneously changing UC voltage. Because the apparent voltage (the voltage measured between the anode and cathode) changes faster than the flowing speed of ions in the electrolyte. Sometimes, a UC voltage appears fully charged, but ions have not fully flowed into the pores of electrodes. If the charging current stops at this time, the apparent voltage will spontaneously decrease and show the real state of charge of the UC. For this reason, UC with the same amount of stored charges can have different voltage values. When the current is larger, this partial charging phenomenon is more prominent.

3) Voltage-dependent impedance: Experiments have proved that UC parameters are voltage and temperature-dependent values [13]. In fact, an UC can be fully charged or discharged operating as an ESS in seconds [14], so UC parameters can be significantly influenced by its voltage. Meanwhile, UC parameters are also influenced by its temperature, especially in extreme environments. However, the modelling of the thermal environment is not the content of this paper, so the operational temperature of UCs is assumed to be perfectly controlled.

III. Modelling Methods for UC

In order to represent these UC dynamics in a time frame of milliseconds, detailed UC modelling methods are studied.

A. RC Ladder Model

RC ladder model or RC transmission line model has a strong physical meaning. It comes from the physical structure of a UC, as shown in Fig. 1. The charges in porous electrodes form numerous distributed capacitors and the equivalent resistance of electrolyte connecting every capacitor [15]. Hence, this RC ladder structure is formed between the anode and cathode of UC, just like a transmission line. However, numerous microscope electric fields are distributed along this equivalent transmission line, and it is impossible to replicate this distribution in an electric circuit model. Therefore, this equivalent transmission is estimated by a finite number of RC circuits, a RC ladder model, as shown in Fig. 2. Since this RC ladder model comes from the physical structure of an UC, it is able to describe the inner charging state of a UC.

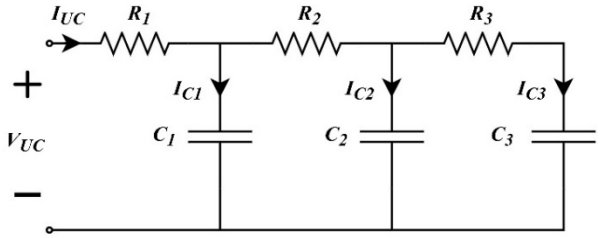

Fig. 2. Structure of RC ladder model.

The RC parameters can be estimated by using a curve-fitting method. Polynomial curves are used to represents the experimental data of a UC. A technology known as electrochemical impedance spectroscopy (EIS) is often used to describe the measured UC impedance. A series of excitation potentials E_0 with a 0.01HZ to 10 kHz sweep frequency are applied on one cell of UC. The resulting current I_0 with a time shift, ϕ is used to calculate the UC impedance as in (1).

$$Z_{UC}(t) = \frac{E_0 \sin(wt)}{I_0 \sin(wt - \phi)} \tag{1}$$

The calculated UC impedance is drawn in a Nyquist plot. The voltage-dependent UC impedance can be observed by measuring the EIS curves of a UC under different voltages. Due to the porous electrodes, the UC resistance is higher at a lower frequency. Since the trajectories are voltage-dependent, the R and C values of a UC can be considered as functions of UC voltage. If the functions for R and C can be formulated, the UC ladder model is determined. The accuracy of curve-fitting is evaluated by the root-mean-square-error (RMSE), which is formulated as,

$$RMSE = \sqrt{\frac{\sum_{i=1}^{N} error_i^2}{N - N_{fitted\ points}}} = \sqrt{\frac{\sum_{i=1}^{N} [(R_{model} - R_{true})^2 + (X_{model} - X_{true})^2]}{N - N_{fitted\ points}}} \tag{2}$$

where N is the total number of impedance points measured in EIS, this RMSE shows the average Euclidean distance between the model curve and the measured curve. A model curve with a smaller RMSE has a better identity than the measured curve. Therefore, the curve-fitting result with minimum RMSE gives the most accurate estimation of UC parameters.

An RC ladder model is often used in the study of UC principles and manufacture rather than power system applications. Because the solution for C1, C2 and C3 voltage has a complex analytical expression which is complicated to be implemented in simulations. Besides, in power system applications, people may prefer to know the state of charge of a whole UC rather than the charge distribution state at the outer layer and inner layer.

B. RC Series-parallel Branch Model

In order to explain the principle of RC series-parallel branch models, the EIS of a UC should be analyzed. As mentioned, the real part of a UC decreases with frequency increasing, which can be recognized as the impedance of porous structure of electrodes named $Z_p(jw)$ [14]. Reference [13] finds an equation to represent the impedance of porous electrodes as,

$$Z_p(jw) = \frac{\tau \cdot \coth\left(\sqrt{jw\tau}\right)}{C_a \cdot \sqrt{jw\tau}} \tag{3}$$

where τ is the time constant of porous electrodes; C_a is the maximum capacitance that can be used in a UC. The time-domain expression of impedance $Z_p(jw)$ can be transformed as (4), which represents the main capacitor C_a in series with infinite numbers of RC parallel branches.

$$\frac{\tau \cdot \coth\left(\sqrt{jw\tau}\right)}{C_a \cdot \sqrt{jw\tau}} \xrightarrow{Time\ dimain} \frac{1}{C_a} + \frac{2}{C_a}\sum_{n=1}^{\infty} e^{-\frac{n^2\pi^2}{\tau}t} \tag{4}$$

By selecting n equals 2, the porous impedance is estimated by two RC parallel branches with time constants $\frac{\tau}{\pi^2}$ and $\frac{\tau}{4\pi^2}$. Then, the parameters of two RC parallel branches are expressed as

$$C_1 = C_2 = \frac{C_a}{2}, R_1 = \frac{2\tau}{\pi^2 C_a}, R_2 = \frac{\tau}{2\pi^2 C_a} \tag{5}$$

where C_1 and C_2 are capacitance of two branches; R_1 and R_2 are the resistance of two branches.

Fig. 3 shows the structure of a three-order RC series-parallel model according to (5). In steady states, all energy is stored in the main capacitor C_a and the voltages of C_1 and C_2 should be 0, which means that the voltage of the capacitor C_a also represents the SOC of this UC. When a charging current I_{UC} is applied on this RC series-parallel model, capacitors C_1 and C_2 are getting charged by currents I_{C1} and I_{C2}. With the increase of C_1 and C_2 voltages, currents I_{C1} and I_{C2} gradually converge to 0. This phenomenon makes the terminal voltage V_{UC} increase faster at the beginning of charging.

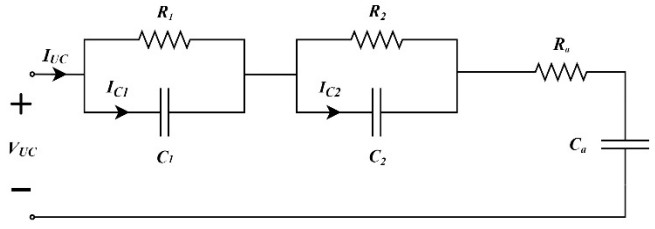

Fig. 3. Structure of RC series-parallel branch model.

The unknown variables are time constant τ and main capacitance C_a, which should be determined by curve-fitting. Similar with the curve-fitting in RC ladder model, polynomial curves are used to estimate the measured impedance curves of EIS. The curve-fitting result with minimum RMSR gives the optimal solution.

C. RC Parallel Branch Model

As the name implies, RC series branches are all in parallel in this model. RC parallel branch model is relatively simpler than RC ladder model on structures. Because the charging state of each RC branch is independently influenced by terminal voltage V_{UC}. One example of RC parallel model is shown in Fig. 4, where the subscripts "f", "d" and "l" stands for fast branch, delayed branch and long-term branch [16]. The fast branch has the smallest resistance and RC time constant, around 20 milliseconds. The delayed branch is relatively slower with a time constant of around 100 seconds, and the long-term branch is the slowest, with a time constant of around 30 minutes. The reason for implementing different time constants of RC branches is to represent distributed elements and charge redistribution. In steady-state, capacitor voltages of three branches equal to the terminal voltage V_{UC}. When terminal voltage V_{UC} changes, due to charging current I_{UC}, the voltage of the fast branch capacitor V_{Cf} changes the fastest to follow the terminal voltage. The delayed branch and long-term branch follow in a longer time scale, which leads to voltage differences between these branches. For this reason, the capacitor voltages will change spontaneously even when external current is removed, which corresponds to the charge redistribution phenomenon.

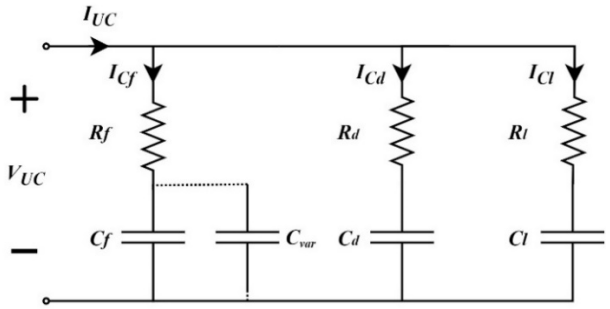

Fig. 4. Structure of RC parallel branch model.

Instead of measuring the EIS of a UC, [17] uses constant current tests to estimate parameter values. Since the time ranges of the three branches are very distinct, a constant current test lasting a specific time can be used to test every branch separately. For example, a current source is switched on for 20ms, and the measured UC voltage can be assumed to be fully influenced by the fast branch because the currents of the delayed branch I_{C_d} and long-term I_{C_l} are very small in 20ms. After determining values for R_f and C_f, the charging time increases to the time scale of the delayed branch and the long-term branch to estimate slow parameters. In order to increase the estimation accuracy of fast UC dynamics, reference [16] adds a variable capacitor at the fast branch. The fast branch capacitor is formed by a constant capacitor C_f and a voltage-dependent capacitor C_{var} which can be expressed as (6), where K_V is the voltage-dependant capacitance constant determined in the constant current test. Since UCs are used for fast active-power response in milliseconds, the behaviour of delayed branch and long-term branch is compromised.

$$C_{var} = K_V \cdot V_{UC} \tag{6}$$

Finally, the RC parallel branch model is selected due to three reasons:

- RC parallel models are based on time scales of UC performance, which also relates to the frequency control performance under different time scopes.
- Fast active power-frequency control focuses on the power response in milliseconds. The fast branch of RC parallel model has a relatively higher accuracy in curve-fitting of UC impedance, which is also in a time scale of milliseconds.

- RC parallel model has a simpler structure. The charging state of every branch are independently determined by terminal voltage V_{UC}. The parameters can be measured separately by constant current tests under different time scales.

IV. UC Model Representation in RSCAD (C-builder)

This paper uses the built-in c-builder function (cf. [17]) available in RSCAD 5.010 to create the UC model for real-time electromagnetic transient (EMT) simulations, since the existing capacitor elements are not suitable to describe the dynamics of an UC. The UC model is represented like a black box, and only important signals are calculated during simulations. C source code determines the actual function of this model. The mathematical representation of an UC model should be written in a C code file. Two physical nodes N_1 and N_2 are defined as the two electrodes. Then, the input values of this UC model are voltages of two electrodes. The output values from the UC model are UC impedance and charging state represented by a conductance value G and a current injection I_{CS} respectively. As a result, the UC model is finally represented as a Norton equivalent form in Fig. 5.

TABLE I. Parameters of RC Parallel Branch Model

Parameters	Values	Parameters	Values
C_f	270F	R_f	2.5mΩ
C_d	100F	R_d	0.5Ω
C_l	220F	R_l	5.2Ω
K_V	190F/V		

The selected parameter values for RC parallel branch model are shown in Table I. In order to simulate this RC parallel branch model in RSCAD, the three RC branches are all represented as Norton form in (8), where G is the conductance value and I_{CS} is the current injection. In every simulation time step Δt, the new values for G and I_{CS} are calculated according to the terminal voltage $V_{UC}(t)$. This is also why three branches can represent different time domains because the charging state of every branch is independently influenced by UC voltage. Besides, the fast branch capacitance is voltage-dependent, which means C_{var} needs to be updated during simulations.

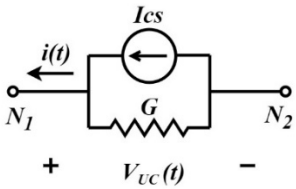

Fig. 5. Norton equivalent form of an UC model.

The mathematical expression of the Norton equivalent circuit is shown in (7). The actual UC voltage variation comes from the integral of UC current. However, the UC current in RTDS is considered as discrete values of simulation time steps. Therefore, the current integral is estimated by a trapezoidal area of UC current between two simulation time steps. The conductance value in (8) is calculated according to the R and C parameters of every branch in Figure 4. The total conductance of the UC model is calculated by summing the conductance of three parallel branches. The current injection I_{CS} of every branch is calculated as (9), which can represent the charging state of the corresponding branch. The value of current injection I_{CS} is determined by the current and voltage of last time step $V_{UC}(t-\Delta t)$ and $i(t-\Delta t)$.

$$i(t) = G \cdot V_{UC}(t) + I_{CS}(t) \tag{7}$$

$$G = \frac{2C}{2RC + \Delta t} \tag{8}$$

$$I_{CS} = -G \cdot V_{UC}(t-\Delta t) + (2RG - 1) \cdot i(t-\Delta t) \tag{9}$$

The G value is represented as a conductance, because it is associated with the current voltage $V(t)$. For the terms in $I_{CS}(t)$, these are all memory values not associated with the current voltage $V(t)$, hence they can be treated as extra current injections in parallel with conductance G. In this way, a capacitor is represented as a conductance in parallel with a time-varying current source, which can participate in RTDS calculations.

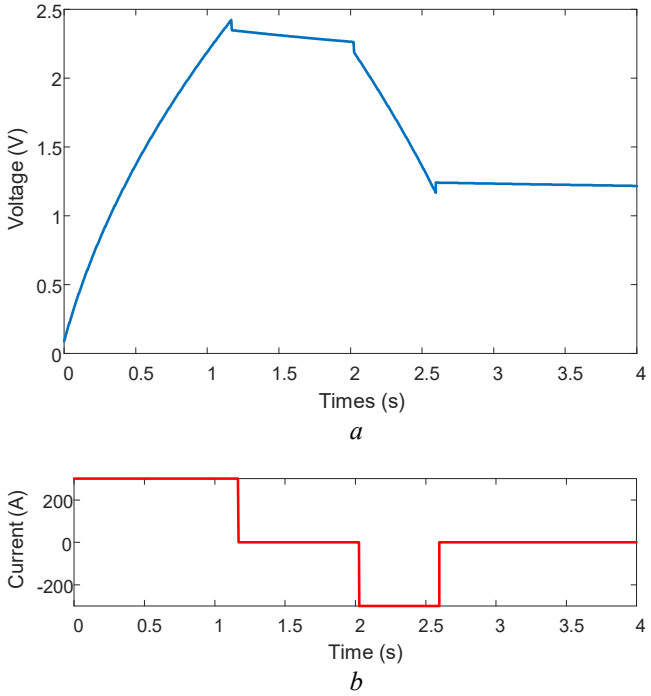

Fig. 6. (a) Terminal voltage of UC model in RTDS. (b) Charging and discharging current for test

The charging curve of the RC parallel branch model is shown in Fig. 6(a). The testing current is shown in Fig. 6(b). The model is first charged with a constant 250A, and the terminal voltage reaches the maximum 2.424V at 1.168s. However, the ramp rate of UC voltage decreases with time, which shows the influence of voltage-dependent capacitance. Later, during the time of zero current, the terminal voltage of UC changes spontaneously, which corresponds to the redistribution phenomenon. The ions in the electrolyte are not entirely located in porous electrodes during the time of charging, and the UC curve during the zero current interval shows the process of still moving ions after charging. Afterwards, the UC model is discharged with a 5A current. The increasing ramp rate of the UC curve proves that UC capacitance is decreasing with voltage value. The voltage curves have step changes at the turning points because resistors share a certain amount of voltage when current flows.

Finally, the UC voltage reaches 1.218V at 4s. The UC voltage will still change in a longer time scale, but it is much longer than the time of fast active power-frequency control. The UC voltage curve shows that the generic UC model in RSCAD is able to describe the studied UC dynamics.

V. Experimental Result

A modified IEEE 9 bus system is used to test the UC performance during fast active power-frequency control. The IEEE 9 bus system and FDWG models are developed in [18]. The 52% of power generation in IEEE 9 bus system is replaced by FDWGs at bus 7 and bus 3 as shown in Figure 7. FDWGs cannot contribute natural inertia to a power system. Therefore, the system inertia is decreased, and the power system frequency becomes more vulnerable to disturbance. Wind power generators are connected to the system through back-to-back converters. The rotor side converter (RSC) is controlled to transfer the maximum amount of power from wind generators. The grid side converter (GSC) is under voltage control to maintain the DC-link voltage constant.

UC and battery combined hybrid energy storage systems shown in Figure 8 are mounted on the DC-link to supply extra power during shortage of generation and support frequency stability. The battery model is shown in the appendix. On one hand, UCs have high power density and fast reacting speed, which can improve the fast active power-frequency response. On the other hand, batteries have higher energy density and lower price, which is suitable to extend the duration of power supply. Meanwhile, UCs can work in severer situations, including rapid changing current, wide temperature range, etc. Hence, UCs can supply a fast power spike and leave the slowly average power to batteries to extend batteries' lifetime.

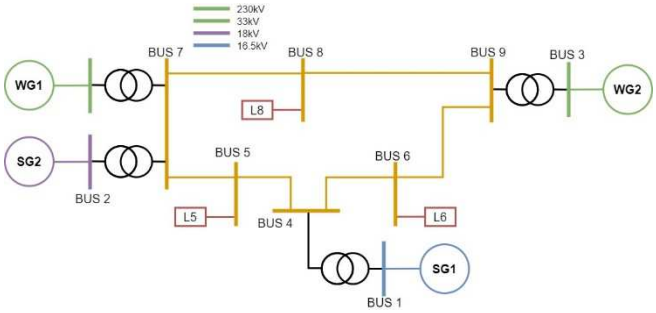

Fig. 7. IEEE 9 bus system with 52% wind generations.

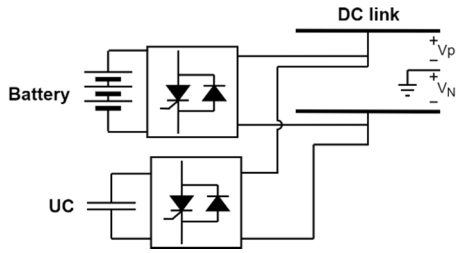

Fig. 8. Hybrid energy storage system connected on the DC link

A load step increase at bus 8 is used to test the frequency stability of this power system. At the beginning of the load increase, more active power is drawn from the kinetic energy of the synchronous generators, which is the reason for the frequency drop. The energy storage systems are connected to the DC-links of FDWG located at bus 7 and bus 9 as the power sources for frequency control. The power balance of synchronous generators will be restored by increasing the power output from FDWGs. In order to prove the advantages of UCs, batteries and UCs based energy storage systems are used, and the droop-derivative control described in [10] is applied in the comparison of their performance. The diagram of droop and derivative control is shown in the appendix. The energy storage and terminal voltage of batteries and UCs are equally dimensioned. Therefore, the difference in their frequency control performance is not influenced by their ratings.

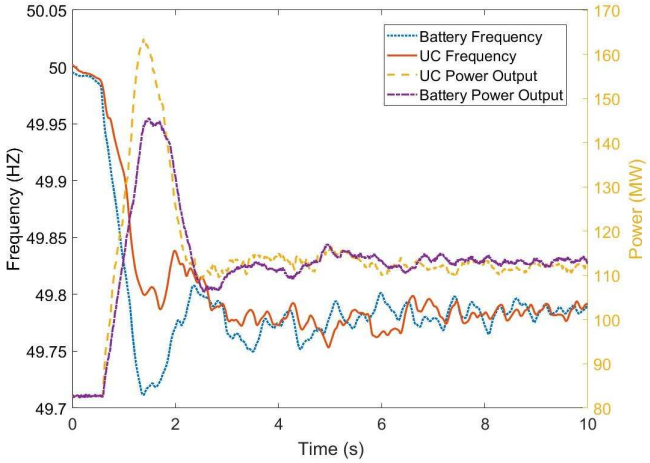

Fig. 9. Frequency performance of batteries and UCs.

A 80 MW load increase is applied on load 8 at 0.5 s. The responses obtained by using UC or battery are shown in Fig. 8. Note that the system frequency starts to drop since the total power generation is lower than the total load demand when the frequency derivative decreases to -0.07HZ/s, the droop-derivative control kicks in. The frequency drop stops within 2s. During this time, the output of droop-derivative control gradually increases to meet the load demand. Finally, the frequency is stabilized around 4s. Since the setting of droop-derivative control is the same for battery and UC, the settled system frequency is the same for two cases, around 49.78HZ. The most significant difference between two cases happens in the first few seconds because the power density and reacting speed of UC is better than the battery. The UC power adjustment is faster than the battery power adjustment. Thus, sufficient power is quickly supplied to effectively prevent the abrupt frequency change when the UC is used. The ROCOF obtained using the UC is 0.225HZ/s, which is lower than the value of ROCOF obtained by using the battery, i.e. 0.309HZ/s. Besides, the resulting maximum frequency deviation is 49.753HZ when the UC is used, which is also better than the value obtained by using the battery, i.e. 49.711HZ.

VI. Conclusions

In this paper, a detailed UC model for real-time simulations is presented. Fast UC dynamics, including distributed circuit elements, charge redistribution and voltage-dependent impedance, are considered due to their influence within the time frame of milliseconds in fast active power-frequency control. The UC model is added to an FDGW, and the performance of this combination is compared with the alternative case when FDGW is combined with an electrical batterie. The qualitative comparison also considers the effect of droop-derivative control, which acts on the UC or the

battery to enhance the fast active-power frequency support by the FDGW. The result shows that UCs can effectively improve the frequency performance, especially the ROCOF, due to the high-power density and fast-reacting speed of UCs. In future work, the optimal design of UC based fast active power-frequency control should be studied to find the maximum extent that UCs are able to improve. Besides, a hybrid energy system can be used to take advantage of both UCs and batteries. Different control strategies (e.g. virtual synchronous power) should also be compared to achieve a faster UC response. Finally, an optimization problem should be formulated to optimally tune the fast active power-frequency controllers and to size the energy storage system.

REFERENCES

[1] S. M. Alhejaj and F. M. Gonzalez-Longatt, "Investigation on grid-scale BESS providing inertial response support," 2016 IEEE International Conference on Power System Technology (POWERCON), Wollongong, NSW, 2016, pp. 1-6.

[2] J. Zhu et al., "Synthetic Inertia Control Strategy for Doubly Fed Induction Generator Wind Turbine Generators Using Lithium-Ion Supercapacitors," in IEEE Transactions on Energy Conversion, vol. 33.

[3] X. Bian, J. Zhang, Y. Ding, J. Zhao, Q. Zhou, and S. Lin, ‘‘Microgrid frequency regulation involving low-wind-speed wind turbine generators based on deep belief network,’’ IET Gener., Transmiss. Distrib., vol. 14, no. 11, pp. 2046–2054, Feb. 2020.

[4] V. Gholamrezaie, M. G. Dozein, H. Monsef, and B. Wu, ‘‘An optimal frequency control method through a dynamic load frequency control (LFC) model incorporating wind farm,’’ IEEE Syst. J., vol. 12, no. 1, pp. 392–401, Mar. 2018.

[5] M. Kheshti, L. Ding, M. Nayeripour, X. Wang, and V. Terzija, ‘‘Active power support of wind turbines for grid frequency events using a reliable power reference scheme,’’ Renew. Energy, vol. 139, pp. 1241–1254, Aug. 2019

[6] W. Bao, L. Ding, Z. Liu, G. Zhu, and V. Terzija, ‘‘Analytically derived fixed termination time for stepwise inertial control of wind turbines—Part I: Analytical derivation,’’ Int. J. Electr. Power Energy Syst., vol. 121, Oct. 2020, Art. no. 106106.

[7] W. Bao, Q. Wu, L. Ding, S. Huang, F. Teng, and V. Terzija, ‘‘Synthetic inertial control of wind farm with BESS based on model predictive control,’’ IET Renew. Power Gener., vol. 14, no. 13, pp. 2447–2455, Oct. 2020.

[8] N. S. Hasan, N. Rosmin, N. M. Nordin, and M. Y. Hassan, ‘‘Virtual inertial support extraction using a super-capacitor for a wind-PMSG application,’’ IET Renew. Power Gener., vol. 13, no. 10, pp. 1802–1808, Jul. 2019.

[9] Y. Liu, W. Du, L. Xiao, H. Wang, and J. Cao, ‘‘A method for sizing energy storage system to increase wind penetration as limited by grid frequency deviations,’’ IEEE Trans. Power Syst., vol. 31, no. 1, pp. 729–737, Jan. 2016.

[10] E. Rakhshani and P. Rodriguez, "Inertia Emulation in AC/DC Interconnected Power Systems Using Derivative Technique Considering Frequency Measurement Effects," in IEEE Transactions on Power Systems, vol. 32, no. 5, pp. 3338-3351, Sept. 2017.

[11] J. Fang, Y. Tang, H. Li and X. Li, "A Battery/Ultracapacitor Hybrid Energy Storage System for Implementing the Power Management of Virtual Synchronous Generators," in IEEE Transactions on Power Electronics, vol. 33, no. 4, pp. 2820-2824, April 2018.

[12] S. Atcitty.Electrochemical capacitor characterization for electric utility applications. PhD thesis, Virginia Tech, 2006.

[13] C. Chiang, J. Yang and W. Cheng, "EKF-based estimation of SOC and temperature in ultracapacitors," 2013 10th IEEE Int. Conf. on Control and Automation (ICCA), Hangzhou, 2013, pp. 274-279.

[14] Akhil, Abbas A., et al. DOE/EPRI 2013 electricity storage handbook in collaboration with NRECA. Albuquerque, NM: Sandia National Laboratories, 2013.

[15] W. Yang, J. E. Carletta, T. T. Hartley and R. J. Veillette, "An ultracapacitor model derived using time-dependent current profiles." 2008 51st Midwest Symposium on Circuits and Systems. IEEE, 2008.

[16] L. Zubieta and R. Bonert, "Characterization of double-layer capacitors (DLCs) for power electronics applications," Conference Record of 1998 IEEE Industry Applications Conference. Thirty-Third IAS Annual Meeting (Cat. No.98CH36242), USA, Vol. 2, 1998.

[17] RTDS Technologies. InRTDS Manuals and Documentation, 2012.

[18] Veera Kumar, Nidarshan. "Real-time simulation based analysis of Fast Active Power Regulation strategies to enhance frequency support from PE interfaced Multi-Energy system.", 2019.

APPENDIX

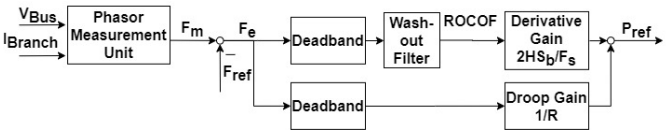

Fig. 10. Diagram of droop and derivative control.

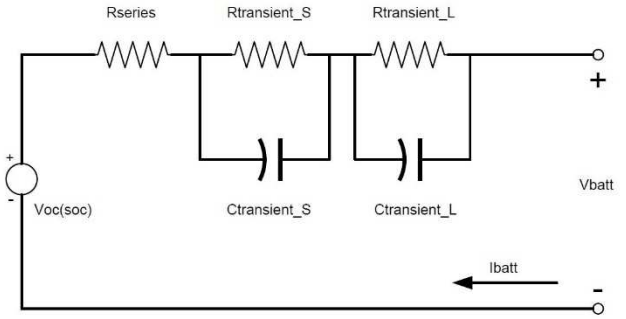

Fig. 11. Structure of battery model.

TABLE II. BATTERY MODEL PARAMETERS

V_{OC}:	$-1.031 \cdot e^{-35 \cdot SOC} + 3.685 + 0.2156 \cdot SOC$ $-0.1178 \cdot SOC^2 + 0.3201 \cdot SOC^3$
R_{series}:	$0.1562 \cdot e^{-24.37 \cdot SOC} + 0.07446$
$R_{Transient\_S}$:	$0.3208 \cdot e^{-29.14 \cdot SOC} + 0.04669$
$C_{Transient\_S}$:	$-752.9 \cdot e^{-13.51 \cdot SOC} + 703.6$
$R_{Transient\_L}$:	$6.603 \cdot e^{-155.2 \cdot SOC} + 0.04984$
$C_{Transient\_L}$:	$-6056 \cdot e^{-27.12 \cdot SOC} + 4475$